Report

Current Biology

FERONIA Receptor Kinase Contributes to Plant Immunity by Suppressing Jasmonic Acid Signaling in *Arabidopsis thaliana*

Highlights

- FERONIA receptor kinase interacts with transcription factor MYC2 in JA signaling
- FERONIA phosphorylates and destabilizes MYC2
- Peptide ligand RALF23 functions through FERONIA to regulate MYC2 and JA signaling

Authors

Hongqing Guo, Trevor M. Nolan, Gaoyuan Song, ..., Patrick S. Schnable, Justin W. Walley, Yanhai Yin

Correspondence

hguo@iastate.edu (H.G.), yin@iastate.edu (Y.Y.)

In Brief

FERONIA receptor kinase plays important roles in growth, development, and stress responses, but the transcription factor(s) mediating FERONIA signaling are not known. Guo et al. establish that the RALF23-FER-MYC2 signaling module is employed by the host plants to regulate coronatine-mediated host susceptibility.

Guo et al., 2018, Current Biology *28*, 1–9
October 22, 2018
https://doi.org/10.1016/j.cub.2018.07.078

CellPress

Please cite this article in press as: Guo et al., FERONIA Receptor Kinase Contributes to Plant Immunity by Suppressing Jasmonic Acid Signaling in *Arabidopsis thaliana*, Current Biology (2018), https://doi.org/10.1016/j.cub.2018.07.078

Current Biology
Report

FERONIA Receptor Kinase Contributes to Plant Immunity by Suppressing Jasmonic Acid Signaling in *Arabidopsis thaliana*

Hongqing Guo,[1,*] Trevor M. Nolan,[1] Gaoyuan Song,[2] Sanzhen Liu,[3,4,5] Zhouli Xie,[1] Jiani Chen,[1,6] Patrick S. Schnable,[3,4] Justin W. Walley,[2] and Yanhai Yin[1,7,*]
[1]Department of Genetics, Development and Cell Biology, Iowa State University, Ames, IA, USA
[2]Department of Plant Pathology and Microbiology, Iowa State University, Ames, IA, USA
[3]Department of Agronomy, Iowa State University, Ames, IA, USA
[4]Data2Bio, Ames, IA 50011-3650, USA
[5]Present address: Department of Plant Pathology, Kansas State University, Manhattan, KS 66506-5502, USA
[6]Present address: Wisconsin Institute for Discovery, University of Wisconsin, 330 N. Orchard Street, Madison, WI 53715, USA
[7]Lead Contact
*Correspondence: hguo@iastate.edu (H.G.), yin@iastate.edu (Y.Y.)
https://doi.org/10.1016/j.cub.2018.07.078

SUMMARY

Bacterial pathogens use effectors and phytotoxins to facilitate infection of host plants. Coronatine (COR) is one of the phytotoxins produced in bacterial pathogens, such as *Pseudomonas syringae* pv. tomato DC3000 (pst DC3000). COR structurally and functionally mimics the active form of the plant hormone jasmonic acid (JA), JA-isoleucine (JA-Ile), and can hijack the host JA-signaling pathway to achieve host disease susceptibility [1]. COR utilizes the transcription factor MYC2, a master regulator of JA signaling, to activate NAC transcription factors, which functions to inhibit accumulation of salicylic acid (SA) and thus compromise host immunity [2]. It has been demonstrated that SA can antagonize JA signaling through NONEXPRESSOR of PATHOGENESIS-RELATED GENE1 (NPR1) [3] and downstream transcription factors TGAs [4] and WRKYs [5, 6]. However, the detailed mechanism by which host plants counteract COR-mediated susceptibility is largely unknown. Here, we show that the receptor kinase FERONIA (FER) functions to inhibit JA and COR signaling by phosphorylating and destabilizing MYC2, thereby positively regulating immunity. Conversely, the peptide ligand RALF23 acts through FER to stabilize MYC2 and elevate JA signaling, negatively contributing to plant immunity. Our results establish the RALF23-FER-MYC2 signaling module and provide a previously unknown mechanism by which host plants utilize FER signaling to counteract COR-mediated host disease susceptibility.

RESULTS AND DISCUSSION

FERONIA (FER) belongs to the CrRLKL1 family of receptor-like kinases and functions in various biological processes, including plant growth, development, hormone signaling, and biotic and abiotic stress responses [7–17]. Several family members are involved in sensing cell wall integrity, mechanical sensing, and pollen tube function [18–24]. A few components in FER-mediated signaling have been described, including peptides RALF1 [25] and RALF23 [26], which function as ligands for FER, and LORELEI (LRE)/LORELEI-LIKE-GPI-ANCHORED PROTEIN 1 (LLG1), which are FER coreceptors [27]. In addition, FER regulates PP2C phosphatase ABI2 to inhibit plant hormone abscisic acid (ABA) signaling [10]. ABI2 dephosphorylates FER, moxt likely as a feedback regulation mechanism [9]. The downstream signaling components, especially transcription factors mediating FER functions, are largely unknown [13, 22, 25].

To understand how FER functions to regulate plant growth and reveal other processes regulated by FER, we performed global gene expression studies with *fer* mutants. RNA sequencing (RNA-seq) analysis indicated that 6,995 genes are differentially expressed (*fer*-DEGs, $q < 0.05$), with 3,127 upregulated and 3,868 downregulated genes in the *fer* mutant, respectively (Figure 1A; Data S1). In order to better understand FER-mediated signaling, we compared *fer*-DEGs with plant hormone-regulated genes. When compared to the genes regulated by growth-promoting hormones, including brassinosteroids (BRs), auxin (IAA), and cytokinin (CK) [30, 31], close correlations were revealed between *fer*-DEGs and genes regulated by BRs (Figure S1A). Specifically, 29.6% of BR-induced genes are downregulated in *fer* and 25.5% BR-repressed genes are upregulated in *fer*, which supports our previous finding that FER is positively involved in BR-regulated plant growth [16].

When compared to the genes regulated by stress-related hormones ABA, salicylic acid (SA), ethylene (ACC), jasmonic acid (JA), and coronatine (COR) [28, 31, 32], a greater degree of overlap was observed between genes upregulated in *fer* and ABA-, JA-, and COR-induced genes and between genes downregulated in *fer* and ABA-, JA-, and COR-repressed genes (Figure 1A). These results indicate that ABA-, JA-, and COR-regulated genes are regulated by FER in an antagonistic manner. For example, 59.8% (482/806 genes) of JA-induced genes are upregulated in *fer* and 44% (309/701 genes) of JA-repressed genes are downregulated in the mutant (Figure 1A). We also tested whether

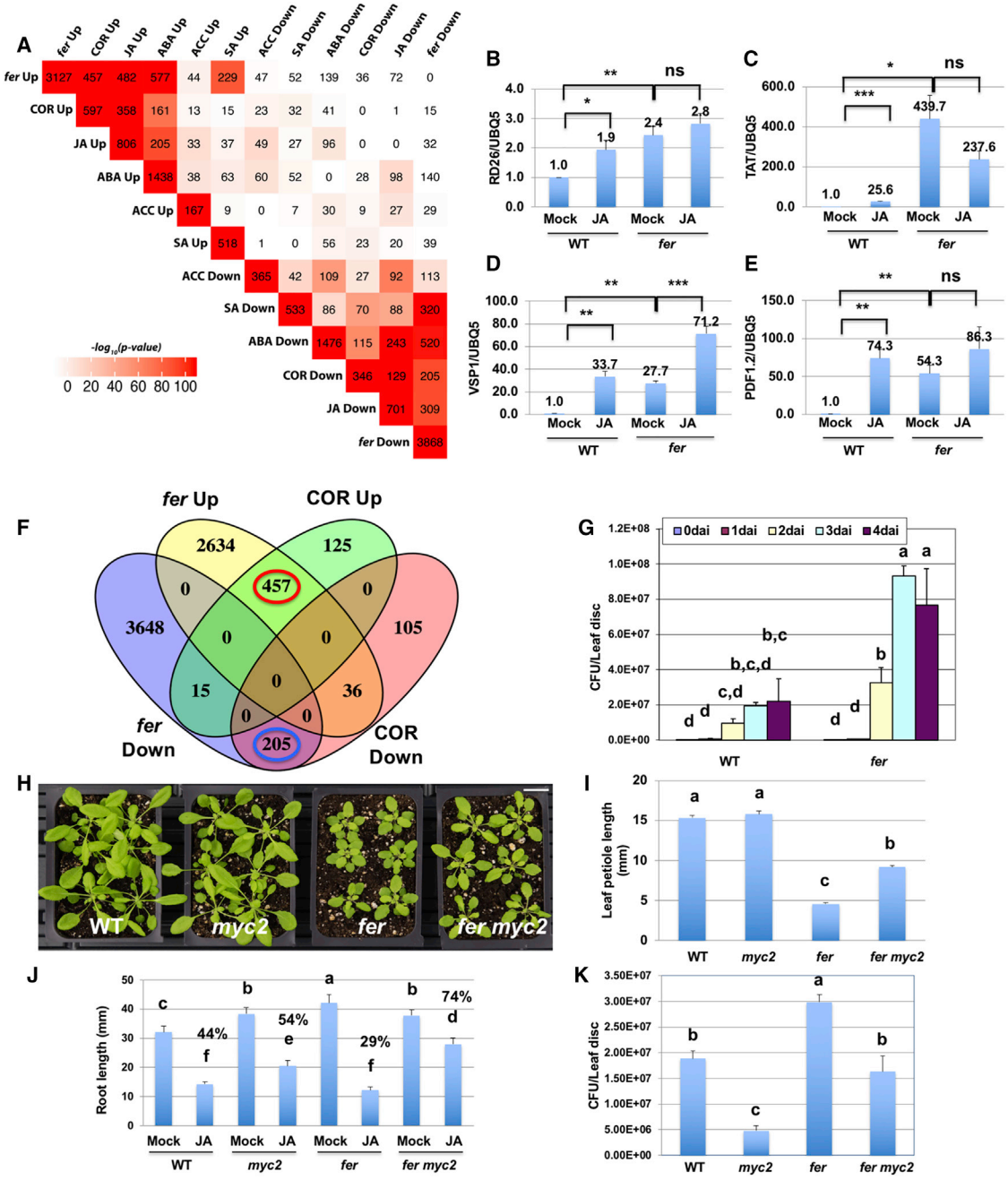

Figure 1. FER Receptor Kinase Functions Upstream of MYC2 to Regulate JA Signaling

(A) Gene expression comparisons among *fer*-DEs and stress hormone-DEs. Color represents −log10 p values from the indicated overlaps calculated from Fisher's exact test by GeneOverlap. The number of genes in each intersection is indicated.

(B–E) The upregulation of several JA-induced genes, *RESPONSIVE TO DESICCATION 26* (*RD26*, B), *TYROSINE AMINO TRANSFERASE* (*TAT*, C), *VEGETATIVE STORAGE PROTEIN 1* (*VSP1*, D) and *PLANT DEFENSIN 1.2* (*PDF1.2*, E), in *fer* and their JA induction were confirmed by qPCR. SE was calculated based on 3 sets of samples per treatment, and Student's t test was used to calculate the statistical significance. *$p < 0.05$, **$p < 0.01$, ***$p < 0.001$, and ns, not significant in Student's t test.

(F) Venn diagram showing overlaps between coronatine-induced (COR Up) or coronatine-repressed genes (COR Down) and genes up- (*fer* Up) or downregulated (*fer* Down) in *fer*. The coronatine-regulated genes were previously published [28], and genes differentially expressed in *fer* were determined by RNA-seq.

(G) *Pseudomonas syringae tomato* DC3000 accumulated more in *fer*. The bacteria were infiltrated into 5-week-old plants, and leaf discs were collected at different days after infiltration (dai). Bacterial accumulation was measured by colony-forming units (CFUs) per leaf disc. Average and SD were calculated from three replicates. The experiments were repeated more than 5 times with similar results [29].

(H and I) Loss-of-function *myc2* mutant suppresses *fer* phenotype in growth as shown with four-week-old plants of WT, *myc2*, *fer*, and *fer myc2* double mutants, bar in (H) represents 2 cm and quantification of the 5th leaf petioles length (average and SE were based on n = 15; I).

(legend continued on next page)

JA-responsive gene expression was altered in *fer* by testing several JA-induced genes via qRT-PCR, using 10-day-old seedlings without or with 50 μM JA treatment. These experiments confirmed that JA-induced genes are constitutively upregulated in *fer*, although the additional increase after JA treatment varied among the genes tested (Figures 1B–1E).

It is well known that COR, a phytotoxin from bacterial pathogens, such as pst DC3000, is structurally similar to JA-isoleucine (JA-Ile) and can activate JA signaling in host plants to achieve host susceptibility [1]. Comparison of *fer*-DEGs and COR-regulated genes shows that more than 75% (713/944 genes) of COR-regulated genes are altered in *fer* mutant. For example, 472 out of 597 COR-induced genes are differentially expressed in *fer*, more than 97% of which (457/472 genes) are upregulated in *fer*. Likewise, 241 out of 347 COR-repressed genes are differentially expressed in *fer*, 85% of which (205/241 genes) are downregulated in the mutant (Figures 1F and S1B). These global gene expression profiles indicate that JA and COR signaling is upregulated in *fer*. A recent report showed that *fer* is more sensitive to DC3000^{COR-} and proposed a positive role of FER in pathogen-associated molecular pattern (PAMP)-triggered immunity (PTI) [26]. Our results indicate that *fer* is also more susceptible to wild-type DC3000 (Figure 1G). Given the striking changes of JA- and COR-regulated genes in *fer*, it is conceivable that elevated JA and COR signaling renders *fer* mutant more prone to the bacterial pathogen infection.

The large number of genes mis-regulated in *fer* suggests that FER regulates diverse biological processes through transcriptional reprogramming. However, knowledge of transcription factors downstream of FER is limited. In order to elucidate the transcription factors involved in controlling *fer*-DEGs, we conducted promoter sequence analysis. The G-box sequence is highly enriched in the promoters of *fer*-DEGs (Figure S1C; Data S1). The G-box exists in many JA target genes and is a binding site for MYC2, a major positive regulator mediating JA and COR signaling [33], suggesting that FER regulates JA- and COR-regulated genes through MYC2. To test the potential interaction of FER and MYC2, we generated a *fer myc2* double mutant and found that *myc2* mutation can partially suppress the *fer* stunted growth phenotype, with longer leaf petioles in the double mutant compared to that of *fer* (Figures 1H and 1I). The partial suppression of *fer* growth phenotype by *myc2* implies that FER regulates additional factors that contribute to growth. Whereas *myc2* is less sensitive to JA in both roots and shoots, *fer* is hypersensitive to JA. *myc2* suppressed *fer* hypersensitivity to JA in *fer myc2* (Figures 1J and S1D–S1H). Additionally, bacterial infection assays showed that *myc2* is more resistant to bacterial infection as reported before [34] and *partially* suppressed the elevated susceptibility of *fer* to DC3000 in the *fer myc2* double mutant (Figure 1K). Together, our genetic studies demonstrate that MYC2 functions downstream of FER and at least partially accounts for the positive role of FER in bacterial defense responses.

The genetic interaction of *FER* and *MYC2* led us to test whether there is a physical interaction between the corresponding proteins. We first tested direct interactions between FER kinase (FERK) domain and MYC2 by glutathione S-transferase (GST) pull-down assays (Figures 2A, 2B, S2A, and S2B). GST-FERK can directly interact with full-length MYC2 and its N terminus (aa 1–251) but very little or not with C terminus (aa 440–623) and the middle region (aa 252–339). Next, the FER-MYC2 interaction was confirmed *in vivo* by co-immunoprecipitation (coIP) and bimolecular fluorescence complementation (BiFC). For these experiments, we employed FERm-GFP, in which the kinase activity is abolished with K565R mutation [17]. The mutation allowed FERm-GFP and MYC2-FLAG to express at high levels in *N. benthamiana* (Figure S2C); thus, we used FERm-GFP for both coIP and the following BiFC experiments. A similar approach has been used to detect interaction between ABI5 and its ubiquitin ligase, KEG, because the interaction could only be detected with mutant KEG [35]. Although the reason for stabilization of FERm-GFP is not known, it is possible that, similar to flagellin receptor FLS2 [36], FER also goes through endocytosis and subsequent degradation upon ligand perception and subsequent activity, which would explain the lower protein level of FER-GFP compared to that of the inactive FERm-GFP. When co-expressed in *N. Benthamiana*, coIP experiments showed that MYC2-FLAG immunoprecipitated with anti-FLAG antibody is associated with FERm-GFP (Figure 2C). Furthermore, BiFC assays with FERm-YFPN and MYC2-YFPC confirmed the interaction between these two proteins and indicated that FER and MYC2 interaction occurs in the cytoplasm (Figure 2D).

The interaction between FER and MYC2 prompted us to test whether FERK can phosphorylate MYC2. *In vitro* kinase assays showed that FERK indeed phosphorylates the full-length as well as the N terminus (N) and middle (M) region of MYC2 (Figures 2E, S2D, and S2E). To test whether FER phosphorylates MYC2 *in vivo*, we generated an anti-MYC2 antibody that recognizes the middle region of MYC2. The antibody recognizes MYC2 in both whole-cell extract and nuclear protein from wild-type (WT) plants, but the signal corresponding to MYC2 protein is absent in *myc2* mutants (Figure S2F). The MYC2 protein from both WT and *fer* was immunoprecipitated by anti-MYC2. Western blotting with anti-phosphoserine showed that MYC2 was phosphorylated in WT, and phosphorylation was reduced in *fer* (Figure 2F), suggesting that MYC2 is phosphorylated by FER *in vivo*.

To determine the effect of FER phosphorylation on MYC2, we examined the MYC2 protein stability in both WT and *fer* mutant with cycloheximide (CHX) treatments. The half-life of MYC2 in WT was around 60 min, and the half-life of the protein was over 120 min in *fer* (Figure 2G). Similar results were obtained in transient assay in *N. benthamiana*. Co-expression of MYC2 with FER, but not FERm, clearly reduced MYC2 protein levels (Figure S2C). These results support the conclusion that FER functions to destabilize MYC2.

(J) The *myc2* suppresses *fer* phenotype in JA inhibition of root growth. Averages and SD were derived from 10–12 seedlings. Percentages of root growth after JA treatment were shown for each genotype. The experiments were repeated more than 3 times with similar results.
(K) The *myc2* suppresses *fer* phenotype in bacterial defense. The experiments were done as described in (G). Average and SE were calculated from three replicates. The experiments were repeated more than 3 times with similar results. Statistical significance was calculated using Tukey HSD test, and p values less than 0.05 were considered significant for (G) and (I)–(K). See also Figure S1, Data S1, and Table S3.

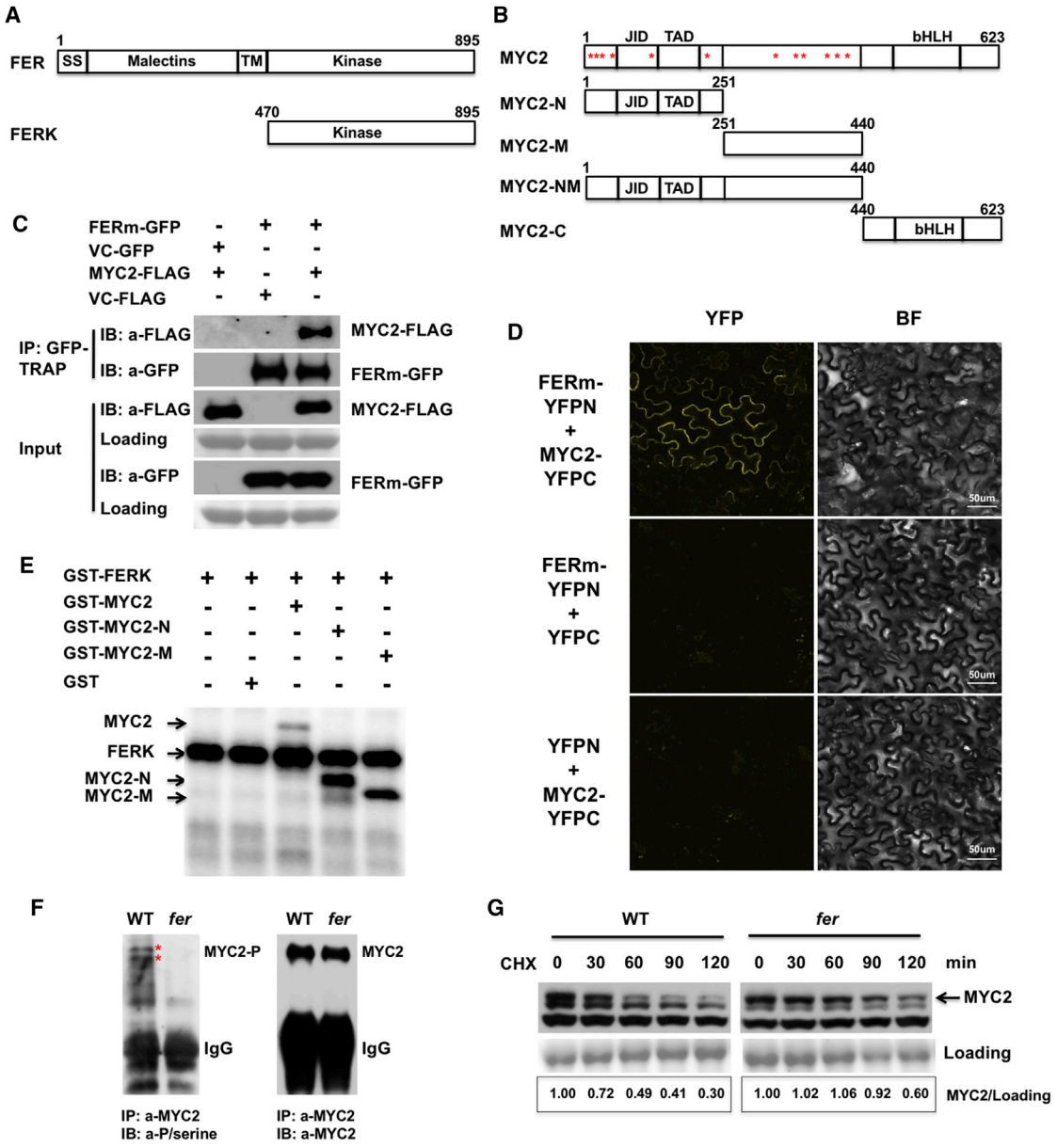

Figure 2. FER Interacts with and Phosphorylates MYC2

(A and B) The domain structures of FER (A) and MYC2 (B) are shown. SS, signal sequence; TM, transmembrane domain. The malectin domains in the extracellular region and FER kinase domain (FERK) are indicated. For MYC2, the amino (N), middle (M), and carboxyl (C) domains used in the study are indicated. Although the C-terminal domain includes basic helix-loop-helix (bHLH) DNA binding motif, the N domain includes JAZ interacting domain (JID) and transcription activation domain (TAD). FER phosphorylation sites are indicted with an asterisk.

(C) FER interacts with MYC2 *in vivo*. MYC2-FLAG and FERm-GFP were co-expressed or each was co-expressed with vector only as controls in *N. Benthamiana* leaves. Total protein was used for immunoprecipitation with GFP-TRAP-MA and detected with anti-GFP or anti-FLAG antibodies. The 1% input from each reaction is shown.

(D) BiFC assay further supports that FER interacts with MYC2 *in vivo*. MYC2 fused with YFP C terminus and FERm fused with YFP N terminus were co-expressed in *N. Benthamiana* leaves, and reconstituted YFP signal was observed in the cytoplasm of epidermal cells. Scale bars represent 50 μm.

(E) FERK phosphorylates full-length, N and M domains of MYC2 in *in vitro* kinase assay. FERK autophosphorylation and various forms of phosphorylated MYC2 are indicated.

(F) MYC2 is phosphorylated in WT, but the phosphorylation is reduced in *fer*. MYC2 was immunoprecipitated from WT and *fer* using anti-MYC2 antibody, and anti-phosphoserine antibody was used to detect MYC2 phosphorylation (left). The detection with anti-MYC2 antibody serves as control (right).

(G) MYC2 has prolonged half-life in *fer* mutant. Ten-day-old seedlings were incubated with MG132 in liquid 1/2 Murashige and Skoog (MS) medium for 16 hr to accumulate MYC2. Then, the seedlings were washed 5 times with 1/2 MS medium to remove MG132 and incubated with cycloheximide (CHX) for indicated times and were collected and flash frozen. Total proteins were extracted and resolved on SDS-PAGE. MYC2 was detected by MYC2 antibody, and Ponceau S staining is used as loading control. Quantification was carried out using ImageJ.

See also Figure S2 and Tables S1, S2, and S3.

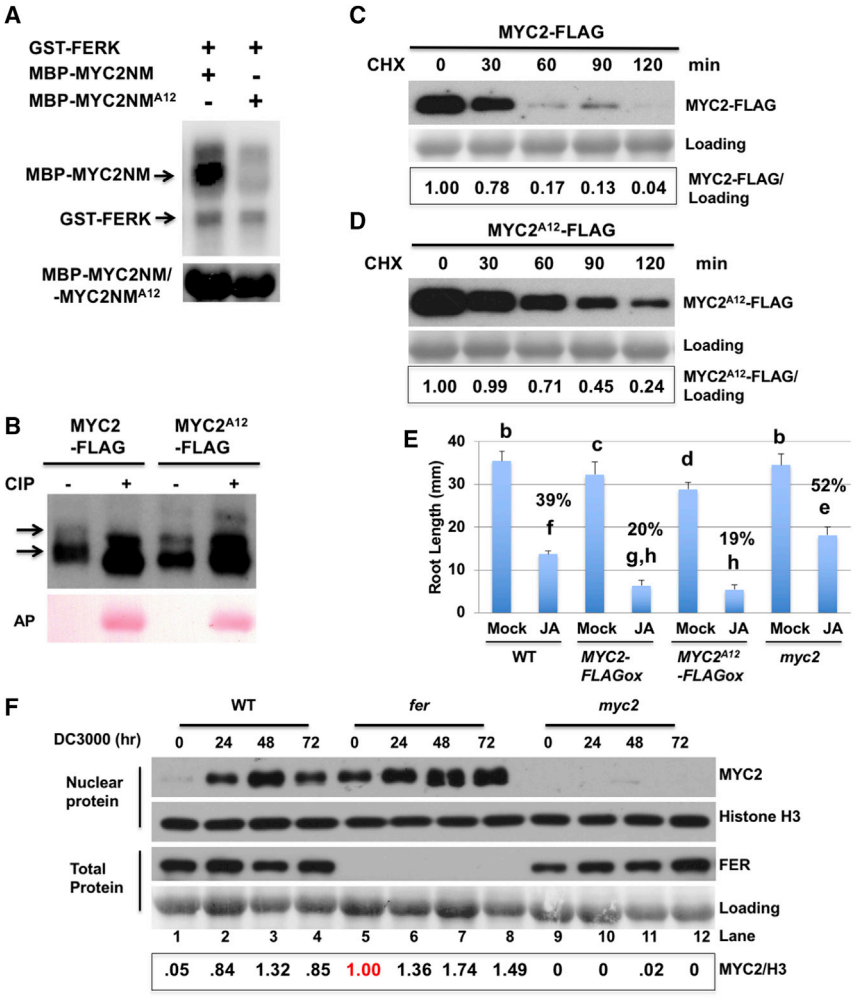

Figure 3. FER Phosphorylation of MYC2 Destabilizes MYC2

(A) FER phosphorylation of MYC2NM (N and middle domains) is reduced when 12 phosphorylation sites are mutated to alanine, indicated as MYC2NM^{A12}. Phosphorylated MYC2NM and FERK autophosphorylation revealed by kinase assay is indicated. The bottom panel indicates MYC2NM and MYC2NM^{A12} used in the assay.

(B) MYC2^{A12} phosphorylation is reduced *in vivo*. MYC2-FLAG and MYC2^{A12}-FLAG were immunoprecipitated from transgenic plants, and the IP product was treated with phosphatase and resolved on a Phos-tag gel. There is a shift in the MYC2-FLAG, and the shift in MYC2^{A12}-FLAG is minimal.

(C and D) MYC2^{A12} has prolonged half-life than that of WT MYC2. Ten-day-old transgenic plants *MYC2-FLAGox* (C) or *MYC2 ^{A12}-FLAGox* (D) were incubated with CHX for indicated times and were collected and flash frozen. Total proteins were extracted and resolved on SDS-PAGE. MYC2-FLAG and MYC2^{A12}-FLAG were detected by anti-FLAG. Ponceau S staining is used as loading control. Quantification was carried out using ImageJ.

(E) Both *MYC2-FLAGox* and *MYC2^{A12}-FLAGox* are hypersensitive to JA in the root growth assay, indicating that MYC2^{A12} is functional (average and SD were calculated based on n = 14–18 plants). Statistical significance was calculated using Tukey HSD test and p values less than 0.05 were considered significant.

(F) MYC2 protein accumulates in *fer* mutant. Five-week-old WT, *fer*, and *myc2* plants were infiltrated with Pst DC3000 for indicated times. Total or nuclear proteins were prepared from each sample, and the accumulation of MYC2 and FER was detected with anti-MYC2 or anti-FER. Anti-Histone H3 and Ponceau S staining were used as loading controls. Quantification of MYC2 was carried out using ImageJ.

See also Figures S2G, S2H, and S3 and Tables S1, S2, and S3.

We then mapped the FER phosphorylation sites on MYC2 using *in vitro* phosphorylated MYC2N and MYC2M via mass spectrometry. In total, 36 possible FER phosphorylation sites were identified, including 6 sites localized to a specific amino acid (Table S1). We chose 12 sites that are mostly conserved among different species (Table S2; Figure 2B) for further mutational analysis. Mutations of these sites to alanine (MYC2 NM^{A12}) largely reduced the FERK phosphorylation of MYC2 N-terminal and middle (NM) domain (Figure 3A).

To further test the effect of the FER phosphorylation of MYC2 on its stability, we generated a mutant form of full-length MYC2, MYC2^{A12}, and obtained stable transgenic *Arabidopsis* plants expressing *MYC2^{A12}-FLAG*. To test the phosphorylation status of MYC2^{A12} in the transgenic plants, immunoprecipitation was carried out using anti-FLAG from the transgenic lines 48 hr post-pst DC3000 infection, and the IP product was treated with alkaline phosphatase and resolved on a Phos-tag gel (Figure 3B). Two forms of MYC2 were observed after blotting with anti-MYC2 antibody, both of which shifted downward after phosphatase treatment in the WT MYC2-FLAG. On the other hand, the effect of the phosphatase treatment on MYC2^{A12}-FLAG was minimal (Figure 3B), suggesting that the mutated amino acids are involved in MYC2 phosphorylation *in vivo*. The different mobility of the two MYC2 forms is most likely due to other post-translational modifications than phosphorylation because both bands were still present after phosphatase treatments.

Next, we carried out cycloheximide treatment with the transgenic lines, which showed that MYC2-FLAG has a half-life between 30 and 60 min (Figure 3C) although MYC2^{A12}-FLAG is more stable, with a half-life of around 90 min (Figure 3D). Similar observations were made in transient assays in *N. Benthamiana*. Whereas MYC2 is clearly reduced by co-expression with FER (Figure S2G, lanes 2, 6, and 10), stabilization of MYC2^{A12} was observed (Figure S2G, lanes 4, 8, and 12), and the stability of MYC2^{A12} was increased 2.7- to 5.3-fold (Figure S2H). Furthermore, treatment with the kinase inhibitor K252a promoted MYC2 accumulation (Figure S2I), confirming that MYC2 stability is related to its phosphorylation.

In order to rule out the possibility that the mutations in MYC2^{A12} rendered the protein dysfunctional, we tested responses to JA and pst DC3000 in MYC2 transgenic lines. Similar to *MYC2-FLAGox*, *MYC2 ^{A12}-FLAGox* also showed

hypersensitivity to JA treatment (Figures 3E and S3A–S3D) and increased pst DC3000 growth (Figure S3E), compared to WT plants, suggesting that $MYC2^{A12}$ is functional in mediating JA responses. Taken together, these data suggest that FER phosphorylation of MYC2 is at least in part responsible for MYC2 destabilization.

With the knowledge that FER phosphorylates and destabilizes MYC2, we hypothesized that the elevated susceptibility of *fer* mutant to pst DC3000 is due to increased levels of MYC2. To test the hypothesis, we infiltrated WT, *fer*, and *myc2* mutant plants with pst DC3000 and examined their MYC2 levels. In WT plants, nuclear MYC2 level is very low and accumulated after bacterial infection, reaching the highest level at 48 hr post-infiltration and declining at 72 hr, with a 35% reduction relative to that of 48 hr (Figure 3F, lanes 1–4). Interestingly, MYC2 accumulated significantly more in *fer* mutant and accumulated even more after bacterial infection, to the highest level at 48 hr post-infiltration with a small decline at 72 hr (Figure 3F, lanes 5–8), consistent with the prolonged half-life of MYC2 in *fer.* As expected, MYC2 was not detected in loss-of-function *myc2* mutants (Figure 3F, lanes 9–12), and FER is absent from *fer* (Figures 3F, lanes 5–8, and S3F). Similar defense response and MYC2 protein changes were also observed in the *amiRNA* knockdown line of FER, *FERamiRNA* [16] (Figures S3G and S3H), confirming that these phenotypes were due to the absence of FER in the *fer* mutants. Furthermore, in transgenic plants expressing FER-GFP, MYC2 induction is greatly reduced 48 hr after pst DC3000 infection, compared to that of WT (Figures S3I and S3J). Taken together, these results demonstrate that pst DC3000 infection induces MYC2 protein in host plants and FER phosphorylates and destabilizes MYC2 to alleviate the pathogen-mediated host disease susceptibility. The increased MYC2 protein levels, both prior and after pathogen infection in *fer*, are at least partially responsible for its compromised immunity.

The peptide hormone RALF1 has been shown to function as a ligand for FER [25]. RALF23 is a homolog of RALF1 and is negatively involved in plant growth [37]. In order to test ligand and receptor relationship of RALF23 and FER, we generated *RALF23ox fer* plants, where *RALF23* is overexpressed in *fer* mutant. *RALF23ox fer* showed a similar growth phenotype to *fer*, indicating that the function of RALF23 is dependent on FER (Figures 4A and S4A).

FER was reported to function as a scaffold protein for PAMP receptors and play a positive role in PTI and plant immunity and that RALF23 functions through FER to negatively regulate PTI and plant immunity [26]. To test whether RALF23 is also involved in MYC2 regulation and JA signaling, we carried out JA response using root growth assays. Similar to the elevated JA sensitivity of *fer*, *RALF23ox* root growth is also hypersensitive to JA treatment (Figures 4B, S3A, S3D, S4B, and S4C). A bacterial infection assay showed that *RALF23ox* accumulated more bacteria than that of WT (Figure 4C), in line with the increased MYC2 protein level (Figure 4D). Moreover, analysis of JA target gene expression in *RALF23ox* showed that some target genes, such as *RD26* and *TAT*, displayed similar patterns of JA response to that in *fer* (Figures 4E and 4F; compare with Figures 1B and 1C), with higher basal expression and additional increase in expression upon JA treatment. Other genes, such as *VSP1* and *PDF1.2*, showed increased JA induction (Figures 4G and 4H), although these genes had lower absolute expression levels in *RALF23ox* compared to WT (Figures S4D and S4E). This phenomenon might be due to complex interactions between FER, MYC2, and other transcription factors in JA target gene regulation. For example, MYC2 and ORA59 negatively regulate each other and potentially negatively regulate each other's target genes (e.g., *VSP1* and *PDF1.2*) [38].

In order to rule out compensatory effects regarding MYC2 levels in *RALF23ox* plants, we tested the short-term effect of RALF23 on MYC2 stability in *N. Benthamiana*. *RALF23-MYC*, used for generating *RALF23ox*, was co-infiltrated with *FER-GFP*, *MYC2-FLAG*, and *S1P-YFP* [39]. S1P, SITE-1 PROTEASE, is required for the production of active RALF23 peptide [26, 37]. Consistent with the increased MYC2 levels in *RALF23ox* plants, accumulation of MYC2-FLAG was observed 48 hr after co-infiltration with *RALF23-MYC*, compared to vector control (Figures 4I, S4F, and S4G). These results demonstrate that both short-term and long-term RALF23 expression lead to increased MYC2 protein accumulation.

To test the effect of RALF23 on MYC2 phosphorylation, we conducted immunoprecipitation with anti-MYC2 from cytoplasmic proteins of *RALF23ox* along with WT and *fer*, treated with pst DC3000 for 48 hr. Because FER interacts with MYC2 in the cytoplasm, we reasoned that we can observe FER-specific MYC2 phosphorylation in cytoplasmic proteins in a less biased way, and pathogen treatment increases MYC2 level so we can circumvent the problem caused by the potential high instability of FER-phosphorylated MYC2. After resolved on a Phos-tag gel, the MYC2 IP showed two distinct forms that are shifted down after alkaline phosphatase treatment, suggesting that MYC2 is phosphorylated and most likely exists in two different forms (Figure S4H), consistent with what we observed with MYC2-FLAG (Figure 3B). The portion of phosphorylated MYC2 protein is decreased in *fer* compared to the non-cytoplasmic MYC2, indicating the phosphorylation is FER-specific. Interestingly, there is only one form of phosphorylated MYC2 observed in *RALF23ox* and the portion of phosphorylated MYC2 is also decreased compared to that of WT, indicating that RALF23 inhibited MYC2 phosphorylation. The difference between *RALF23ox* and *fer* might be due to RALF23's regulation on FER homologs that are potentially involved in MYC2 phosphorylation as well. The results suggest that RALF23 functions through FER to play a positive role in JA signaling and negative role in plant immunity by suppressing FER function and elevating MYC2 levels. We also observed that FER protein level is decreased in *RALF23ox*, which provides another form of regulation of FER by RALF23 (Figure S4I).

In summary, our results demonstrate that FER negatively regulates JA and COR signaling and positively contributes to plant immunity, which establishes FER as a critical regulator of JA and COR signaling and provides a novel mechanism that host plants possess to counteract COR-mediated MYC2 elevation (Figure S4J) and disease susceptibility. It has recently been reported that RALF23 functions through FER to negatively regulate PTI and plant immunity [26]. It is conceivable that RALF23/FER-mediated signaling pathway employs different means to regulate both host plant disease susceptibility through MYC2 and defense responses through PTI. Our study thus establishes

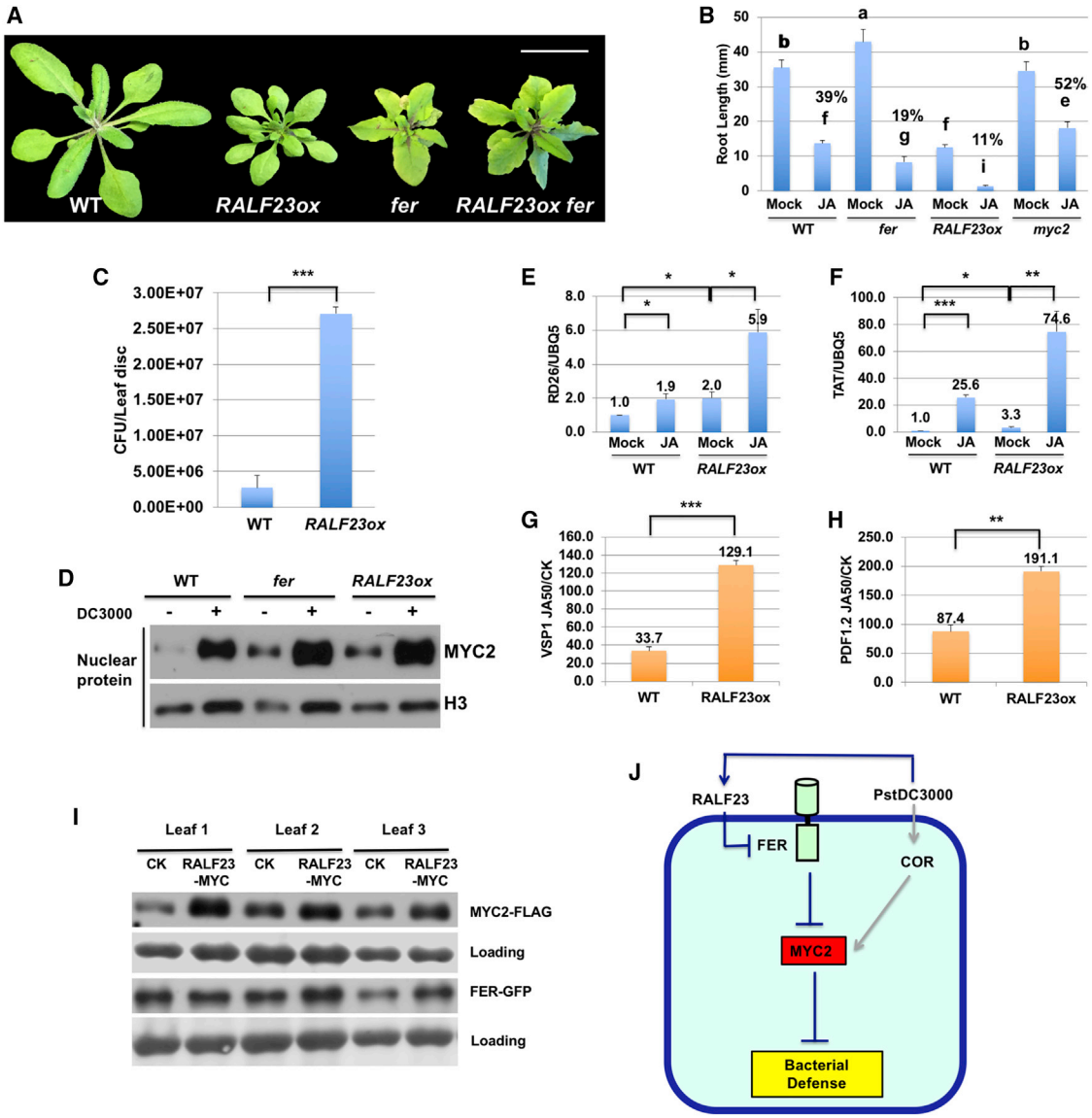

Figure 4. FER Regulation of MYC2 and Modulation by RALF23

(A) Four-week-old plants show growth phenotypes of WT, *RALF23ox*, *fer*, and *RALF23ox fer*. Scale bar represents 2 cm.

(B) *RALF23ox* plants are more sensitive to JA inhibition of root growth; average and SD were calculated from 14–18 seedlings. Statistical significance was calculated using Tukey HSD test, and p values less than 0.05 were considered significant (n = 14–18).

(C) *RALF23ox* plants are more susceptible to bacterial infection. The experiment is described in Figure 1G. Average and SD were calculated from 3 replicates. The statistical significance is evaluated by Student's t test; ***$p < 0.001$ (n = 3). The experiment was repeated three times with similar results.

(D) *RALF23ox* plants accumulate more MYC2 in response to pst DC3000 than WT control. Four-week-old plants with the indicated genotypes were infiltrated with Pst DC3000 for 2 days, and nuclear protein was prepared and blotted with anti-MYC2 or anti-histone H3.

(E–H) Relative JA target gene expression analysis in *RALF23ox* shows that RALF23 plays an important role in JA signaling: *RD26/UBQ5* (B), *TAT/UBQ5* (C), *VSP1* induction by 50 μM JA (JA50/CK, D) and *PDF1.2* induction by 50 μM JA (JA50/CK, E). RNA was prepared from 10-day-old WT or *RALF23ox* seedlings with or without 50 μM JA, and qPCR was performed with the indicated genes. SE was calculated based on 3 sets of samples per treatment, and Student's t test was used to calculate the statistical significance. *$p < 0.05$, **$p < 0.01$, ***$p < 0.001$.

(I) Similar to the effect of RALF23 on MYC2 in *RALF23ox*, short-term RALF23 treatment also promotes MYC2 stability. FER-GFP, MYC2-FLAG, and S1P-YFP were co-expressed with RALF23 or vector only for 48 hr. Total protein was extracted from leaf discs and resolved on SDS-PAGE. All three leaves assayed showed elevated MYC2 level.

(J) A working model for FER and RALF23 regulation of MYC2 during pst DC3000 infection. FER phosphorylates and inhibits MYC2 to positively contribute to plant defense. RALF23 peptide, the processing of which is increased by bacterial infection, functions to inhibit FER receptor signaling hence negatively contributes to bacterial defense.

See also Figures S3A, S3D, and S4 and Table S3.

a more comprehensive signaling pathway from a peptide ligand (RALF23) to its receptor (FER) and downstream transcription factor (MYC2) in the regulation of JA and COR signaling and plant responses to bacterial pathogen infection (Figure 4J).

In addition to FER's role as a negative regulator in JA signaling, our global gene expression data also indicate that FER functions to suppress many other hormone-regulated stress responses. Future studies of the crosstalk between FER signaling and hormonal pathways will reveal more complete mechanisms by which FER regulates plant growth and stress responses.

STAR★METHODS

Detailed methods are provided in the online version of this paper and include the following:

- KEY RESOURCES TABLE
- CONTACT FOR REAGANT AND RESOURCE SHARING
- EXPERIMENTAL MODEL AND SUBJECT DETAILS
  - Plant Materials and Growth Conditions
- METHOD DETAILS
  - RNA-seq
  - Bacterial pathogen growth and infiltration
  - Jasmonic acid treatment
  - Total protein and nuclear protein extraction
  - Protein half-life determination
  - Transient expression assay in Nicotiana benthamiana (N. benthamiana)
  - Co-immunoprecipitation (CoIP)
  - BiFC Assay
  - Immunoprecipitation (IP) and *in vivo* phosphorylation detection
  - *In vitro* GST pull-down assay
  - *In vitro* kinase assay and Mass Spectrometry to identify FER phosphorylation sites on MYC2
  - Antibody Production
- QUANTIFICATION AND STATISTICAL ANALYSIS
  - RNA-seq data analysis
  - Root length measurement
- DATA AND SOFTWARE AVAILABILITY

SUPPLEMENTAL INFORMATION

Supplemental Information includes four figures, three tables, and one data file and can be found with this article online at https://doi.org/10.1016/j.cub.2018.07.078.

ACKNOWLEDGMENTS

H.G. would like to thank Prof. Jo Anne Powell-Coffman and Prof. Steve Whitham for guidance and encouragement, Dr. Bing Yang for pst DC3000, and Dr. Ping He and Dr. Libo Shan for pst DC3000^{COR-}. The research is supported by Signature Research Initiative of the College of Liberal Arts and Sciences and Plant Sciences Institute of Iowa State University.

AUTHOR CONTRIBUTIONS

H.G. and Y.Y. conceived the project. H.G. performed most of the genetic, molecular, and biochemical experiments. T.M.N. performed confocal microscopy experiments and gene expression comparisons and assisted with mapping MYC2 phosphorylation sites. S.L. and P.S.S. performed RNA-seq analysis. G.S. and J.W.W. performed mass spectrometry and analysis. Z.X. performed GST pull-down assay, and J.C. generated FER antibody. All authors contributed to analysis of corresponding data. H.G. wrote the paper with edits from other co-authors.

DECLARATION OF INTERESTS

S.L. and P.S.S. are shareholders of Data2Bio, Ames, IA, USA. H.G. and Y.Y. are co-inventors on the patent US9512440B2, titled "Modulation of receptor-like kinases for promotion of plant growth."

Received: November 14, 2017
Revised: June 28, 2018
Accepted: July 30, 2018
Published: September 27, 2018

REFERENCES

1. Xin, X.F., and He, S.Y. (2013). Pseudomonas syringae pv. tomato DC3000: a model pathogen for probing disease susceptibility and hormone signaling in plants. Annu. Rev. Phytopathol. *51*, 473–498.
2. Zheng, X.Y., Spivey, N.W., Zeng, W., Liu, P.P., Fu, Z.Q., Klessig, D.F., He, S.Y., and Dong, X. (2012). Coronatine promotes Pseudomonas syringae virulence in plants by activating a signaling cascade that inhibits salicylic acid accumulation. Cell Host Microbe *11*, 587–596.
3. Spoel, S.H., Koornneef, A., Claessens, S.M., Korzelius, J.P., Van Pelt, J.A., Mueller, M.J., Buchala, A.J., Métraux, J.P., Brown, R., Kazan, K., et al. (2003). NPR1 modulates cross-talk between salicylate- and jasmonate-dependent defense pathways through a novel function in the cytosol. Plant Cell *15*, 760–770.
4. Zander, M., La Camera, S., Lamotte, O., Métraux, J.P., and Gatz, C. (2010). Arabidopsis thaliana class-II TGA transcription factors are essential activators of jasmonic acid/ethylene-induced defense responses. Plant J. *61*, 200–210.
5. Mao, P., Duan, M., Wei, C., and Li, Y. (2007). WRKY62 transcription factor acts downstream of cytosolic NPR1 and negatively regulates jasmonate-responsive gene expression. Plant Cell Physiol. *48*, 833–842.
6. Li, J., Brader, G., and Palva, E.T. (2004). The WRKY70 transcription factor: a node of convergence for jasmonate-mediated and salicylate-mediated signals in plant defense. Plant Cell *16*, 319–331.
7. Yu, Y., Chakravorty, D., and Assmann, S.M. (2018). The G protein β-subunit, AGB1, interacts with FERONIA in RALF1-regulated stomatal movement. Plant Physiol. *176*, 2426–2440.
8. Feng, W., Kita, D., Peaucelle, A., Cartwright, H.N., Doan, V., Duan, Q., Liu, M.C., Maman, J., Steinhorst, L., Schmitz-Thom, I., et al. (2018). The FERONIA receptor kinase maintains cell-wall integrity during salt stress through Ca2+ signaling. Curr. Biol. *28*, 666–675.e5.
9. Chen, J., Yu, F., Liu, Y., Du, C., Li, X., Zhu, S., Wang, X., Lan, W., Rodriguez, P.L., Liu, X., et al. (2016). FERONIA interacts with ABI2-type phosphatases to facilitate signaling cross-talk between abscisic acid and RALF peptide in Arabidopsis. Proc. Natl. Acad. Sci. USA *113*, E5519–E5527.
10. Yu, F., Qian, L., Nibau, C., Duan, Q., Kita, D., Levasseur, K., Li, X., Lu, C., Li, H., Hou, C., et al. (2012). FERONIA receptor kinase pathway suppresses abscisic acid signaling in Arabidopsis by activating ABI2 phosphatase. Proc. Natl. Acad. Sci. USA *109*, 14693–14698.
11. Kessler, S.A., Shimosato-Asano, H., Keinath, N.F., Wuest, S.E., Ingram, G., Panstruga, R., and Grossniklaus, U. (2010). Conserved molecular components for pollen tube reception and fungal invasion. Science *330*, 968–971.
12. Keinath, N.F., Kierszniowska, S., Lorek, J., Bourdais, G., Kessler, S.A., Shimosato-Asano, H., Grossniklaus, U., Schulze, W.X., Robatzek, S., and Panstruga, R. (2010). PAMP (pathogen-associated molecular pattern)-induced changes in plasma membrane compartmentalization reveal novel components of plant immunity. J. Biol. Chem. *285*, 39140–39149.
13. Duan, Q., Kita, D., Li, C., Cheung, A.Y., and Wu, H.M. (2010). FERONIA receptor-like kinase regulates RHO GTPase signaling of root hair development. Proc. Natl. Acad. Sci. USA *107*, 17821–17826.

14. Deslauriers, S.D., and Larsen, P.B. (2010). FERONIA is a key modulator of brassinosteroid and ethylene responsiveness in Arabidopsis hypocotyls. Mol. Plant *3*, 626–640.
15. Guo, H., Ye, H., Li, L., and Yin, Y. (2009). A family of receptor-like kinases are regulated by BES1 and involved in plant growth in Arabidopsis thaliana. Plant Signal. Behav. *4*, 784–786.
16. Guo, H., Li, L., Ye, H., Yu, X., Algreen, A., and Yin, Y. (2009). Three related receptor-like kinases are required for optimal cell elongation in Arabidopsis thaliana. Proc. Natl. Acad. Sci. USA *106*, 7648–7653.
17. Escobar-Restrepo, J.M., Huck, N., Kessler, S., Gagliardini, V., Gheyselinck, J., Yang, W.C., and Grossniklaus, U. (2007). The FERONIA receptor-like kinase mediates male-female interactions during pollen tube reception. Science *317*, 656–660.
18. Schoenaers, S., Balcerowicz, D., Breen, G., Hill, K., Zdanio, M., Mouille, G., Holman, T.J., Oh, J., Wilson, M.H., Nikonorova, N., et al. (2018). The auxin-regulated CrRLK1L kinase ERULUS controls cell wall composition during root hair tip growth. Curr. Biol. *28*, 722–732.e6.
19. Mang, H., Feng, B., Hu, Z., Boisson-Dernier, A., Franck, C.M., Meng, X., Huang, Y., Zhou, J., Xu, G., Wang, T., et al. (2017). Differential regulation of two-tiered plant immunity and sexual reproduction by ANXUR receptor-like kinases. Plant Cell *29*, 3140–3156.
20. Ge, Z., Bergonci, T., Zhao, Y., Zou, Y., Du, S., Liu, M.C., Luo, X., Ruan, H., García-Valencia, L.E., Zhong, S., et al. (2017). *Arabidopsis* pollen tube integrity and sperm release are regulated by RALF-mediated signaling. Science *358*, 1596–1600.
21. Shih, H.W., Miller, N.D., Dai, C., Spalding, E.P., and Monshausen, G.B. (2014). The receptor-like kinase FERONIA is required for mechanical signal transduction in Arabidopsis seedlings. Curr. Biol. *24*, 1887–1892.
22. Boisson-Dernier, A., Lituiev, D.S., Nestorova, A., Franck, C.M., Thirugnanarajah, S., and Grossniklaus, U. (2013). ANXUR receptor-like kinases coordinate cell wall integrity with growth at the pollen tube tip via NADPH oxidases. PLoS Biol. *11*, e1001719.
23. Boisson-Dernier, A., Roy, S., Kritsas, K., Grobei, M.A., Jaciubek, M., Schroeder, J.I., and Grossniklaus, U. (2009). Disruption of the pollen-expressed FERONIA homologs ANXUR1 and ANXUR2 triggers pollen tube discharge. Development *136*, 3279–3288.
24. Hématy, K., Sado, P.E., Van Tuinen, A., Rochange, S., Desnos, T., Balzergue, S., Pelletier, S., Renou, J.P., and Höfte, H. (2007). A receptor-like kinase mediates the response of Arabidopsis cells to the inhibition of cellulose synthesis. Curr. Biol. *17*, 922–931.
25. Haruta, M., Sabat, G., Stecker, K., Minkoff, B.B., and Sussman, M.R. (2014). A peptide hormone and its receptor protein kinase regulate plant cell expansion. Science *343*, 408–411.
26. Stegmann, M., Monaghan, J., Smakowska-Luzan, E., Rovenich, H., Lehner, A., Holton, N., Belkhadir, Y., and Zipfel, C. (2017). The receptor kinase FER is a RALF-regulated scaffold controlling plant immune signaling. Science *355*, 287–289.
27. Li, C., Yeh, F.L., Cheung, A.Y., Duan, Q., Kita, D., Liu, M.C., Maman, J., Luu, E.J., Wu, B.W., Gates, L., et al. (2015). Glycosylphosphatidylinositol-anchored proteins as chaperones and co-receptors for FERONIA receptor kinase signaling in Arabidopsis. eLife *4*, e06587.
28. Thilmony, R., Underwood, W., and He, S.Y. (2006). Genome-wide transcriptional analysis of the Arabidopsis thaliana interaction with the plant pathogen Pseudomonas syringae pv. tomato DC3000 and the human pathogen Escherichia coli O157:H7. Plant J. *46*, 34–53.
29. Bailey, T.L. (2011). DREME: motif discovery in transcription factor ChIP-seq data. Bioinformatics *27*, 1653–1659.
30. Ye, H., Liu, S., Tang, B., Chen, J., Xie, Z., Nolan, T.M., Jiang, H., Guo, H., Lin, H.Y., Li, L., et al. (2017). RD26 mediates crosstalk between drought and brassinosteroid signalling pathways. Nat. Commun. *8*, 14573.
31. Nemhauser, J.L., Hong, F., and Chory, J. (2006). Different plant hormones regulate similar processes through largely nonoverlapping transcriptional responses. Cell *126*, 467–475.
32. Pajerowska-Mukhtar, K.M., Wang, W., Tada, Y., Oka, N., Tucker, C.L., Fonseca, J.P., and Dong, X. (2012). The HSF-like transcription factor TBF1 is a major molecular switch for plant growth-to-defense transition. Curr. Biol. *22*, 103–112.
33. Kazan, K., and Manners, J.M. (2013). MYC2: the master in action. Mol. Plant *6*, 686–703.
34. Laurie-Berry, N., Joardar, V., Street, I.H., and Kunkel, B.N. (2006). The Arabidopsis thaliana JASMONATE INSENSITIVE 1 gene is required for suppression of salicylic acid-dependent defenses during infection by Pseudomonas syringae. Mol. Plant Microbe Interact. *19*, 789–800.
35. Liu, H., and Stone, S.L. (2013). Cytoplasmic degradation of the Arabidopsis transcription factor abscisic acid insensitive 5 is mediated by the RING-type E3 ligase KEEP ON GOING. J. Biol. Chem. *288*, 20267–20279.
36. Robatzek, S., Chinchilla, D., and Boller, T. (2006). Ligand-induced endocytosis of the pattern recognition receptor FLS2 in Arabidopsis. Genes Dev. *20*, 537–542.
37. Srivastava, R., Liu, J.X., Guo, H., Yin, Y., and Howell, S.H. (2009). Regulation and processing of a plant peptide hormone, AtRALF23, in Arabidopsis. Plant J. *59*, 930–939.
38. Wasternack, C., and Hause, B. (2013). Jasmonates: biosynthesis, perception, signal transduction and action in plant stress response, growth and development. An update to the 2007 review in Annals of Botany. Ann. Bot. *111*, 1021–1058.
39. Liu, J.X., Srivastava, R., Che, P., and Howell, S.H. (2007). Salt stress responses in Arabidopsis utilize a signal transduction pathway related to endoplasmic reticulum stress signaling. Plant J. *51*, 897–909.
40. Yu, X., Li, L., Li, L., Guo, M., Chory, J., and Yin, Y. (2008). Modulation of brassinosteroid-regulated gene expression by Jumonji domain-containing proteins ELF6 and REF6 in Arabidopsis. Proc. Natl. Acad. Sci. USA *105*, 7618–7623.
41. Lu, D., Lin, W., Gao, X., Wu, S., Cheng, C., Avila, J., Heese, A., Devarenne, T.P., He, P., and Shan, L. (2011). Direct ubiquitination of pattern recognition receptor FLS2 attenuates plant innate immunity. Science *332*, 1439–1442.
42. Alonso, J.M., Stepanova, A.N., Leisse, T.J., Kim, C.J., Chen, H., Shinn, P., Stevenson, D.K., Zimmerman, J., Barajas, P., Cheuk, R., et al. (2003). Genome-wide insertional mutagenesis of Arabidopsis thaliana. Science *301*, 653–657.
43. Katagiri, F., Thilmony, R., and He, S.Y. (2002). The Arabidopsis thaliana-pseudomonas syringae interaction. Arabidopsis Book *1*, e0039.
44. Xu, F., and Copeland, C. (2012). Nuclear extraction from Arabidopsis thaliana. Bio-protocol *2*, e306.
45. Jung, C., Zhao, P., Seo, J.S., Mitsuda, N., Deng, S., and Chua, N.H. (2015). PLANT U-BOX PROTEIN10 regulates MYC2 stability in Arabidopsis. Plant Cell *27*, 2016–2031.
46. Nolan, T.M., Brennan, B., Yang, M., Chen, J., Zhang, M., Li, Z., Wang, X., Bassham, D.C., Walley, J., and Yin, Y. (2017). Selective autophagy of BES1 mediated by DSK2 balances plant growth and survival. Dev. Cell *41*, 33–46.e7.
47. Yin, Y., Wang, Z.Y., Mora-Garcia, S., Li, J., Yoshida, S., Asami, T., and Chory, J. (2002). BES1 accumulates in the nucleus in response to brassinosteroids to regulate gene expression and promote stem elongation. Cell *109*, 181–191.
48. Chalkley, R.J., and Clauser, K.R. (2012). Modification site localization scoring: strategies and performance. Mol. Cell. Proteomics *11*, 3–14.
49. Wu, T.D., and Nacu, S. (2010). Fast and SNP-tolerant detection of complex variants and splicing in short reads. Bioinformatics *26*, 873–881.
50. Bullard, J.H., Purdom, E., Hansen, K.D., and Dudoit, S. (2010). Evaluation of statistical methods for normalization and differential expression in mRNA-seq experiments. BMC Bioinformatics *11*, 94.
51. Nettleton, D., Hwang, J.T.G., Caldo, R.A., and Wise, R.P. (2006). Estimating the number of true null hypotheses from a histogram of p values. J. Agric. Biol. Environ. Stat. *11*, 337–356.
52. Benjamini, Y., and Hochberg, Y. (1995). Controlling the false discovery rate: a practical and powerful approach to multiple testing. J. R. Stat. Soc. B *57*, 289–300.

STAR★METHODS

KEY RESOURCES TABLE

REAGENT or RESOURCE	SOURCE	IDENTIFIER
Antibodies		
Rabbit polyclonal anti-FLAG	Sigma-Aldrich	Cat# F7425; RRID: AB_439687
Rabbit polyclonal anti-GFP	[40]	N/A
GFP-TRAP-MA	Chromotek	Cat# GFP-Trap MA
Mouse monoclonal anti-phosphoserine	Sigma-Aldrich	Cat# P3430; RRID: AB_477336
Rabbit polyclonal anti-MYC2	This study	N/A
Rabbit polyclonal anti-FER	This study	N/A
Mouse monoclonal anti-Histone H3	Sigma-Aldrich	CAT# SAB4200651
Rabbit polyclonal anti-c-MYC	Sigma-Aldrich	Cat#C3956; RRID: AB_439680
Mouse monoclonal anti-MBP	New England Biolabs	Cat#E8032; RRID: AB_1559730
Goat anti-rabbit IgG-HRP secondary antibody	Thermo Fisher	Cat#31460
Sheep anti-mouse IgG-HRP secondary antibody	Sigma-Aldrich	GENXA931-1ML
Bacterial and Virus Strains		
E.coli T1	N/A	N/A
E. coli BL21 Gold (DE3)	Thermo Fisher	Cat#50-125-348
Agrobacterium tumefaciens (strain GV3101)	N/A	N/A
Psedomonas synringae pv. Tomato DC3000	Dr. Bing Yang	N/A
Psedomonas synringae pv. Tomato DC3000 $^{Cor-}$	Dr. Ping He	N/A
Chemicals, Peptides, and Recombinant Proteins		
MG132	Sigma-Aldrich	Cat#M7449
Cycloheximide	Sigma-Aldrich	Cat#C4859
Complete protease inhibitor cocktail tablets	Sigma-Aldrich	Cat#11836170001
Trizol	Thermo Fisher	Cat#15596018
RNeasy Kit	QIAGEN	Cat#74904
Phos-tag reagent	Wako	Cat#ALL-107
Linsmaier and Skoog	Caisson Laboratories	Cat#LPS03-1LT
Dynabeads Protein A	Thermo Fisher	Cat#00354691
Jasmonic Acid	Sigma-Aldrich	Cat#J2500
Glutathione HiCap Matrix	QIAGEN	Cat#30900
Amylose Resin	New England Biolabs	Cat#E8021S
Anti-FLAG M2 Magnetic Beads	Sigma-Aldrich	Cat#M8823-1ML
Glu-C	Thermo Fisher	Cat#90054
Trypsin	Roche	Cat#03708969001
Ponceau S	Sigma-Aldrich	Cat#P7170-1L
K252a	Sigma-Aldrich	Cat#K2015-200ul
Halt protease and phosphatase inhibitor cocktail	Thermo Fisher	Cat#78440
Alkaline phosphatatse	Sigma-Aldrich	Cat#P7923-2KU
Deposited Data		
Raw data files for RNA sequencing	NCBI Sequence Read Archive	SRA: PRJNA215313 (https://www.ncbi.nlm.nih.gov/biosample?LinkName=bioproject_biosample_all&from_uid=2318102.)
Raw mass spectra	ID: MSV000080972 Password: MYC2	ftp://MSV000080972@massive.ucsd.edu

(*Continued on next page*)

Continued

REAGENT or RESOURCE	SOURCE	IDENTIFIER
Experimental Models: Organisms/Strains		
E. coli BL21 Gold (DE3)	Thermo Fisher	Cat#50-125-348
Agrobacterium tumefaciens (strain GV3101)	N/A	N/A
Psedomonas synringae pv. Tomato DC3000	Dr. Bing Yang	N/A
Psedomonas synringae pv. Tomato DC3000 $^{Cor-}$	Dr. Ping He	N/A
Nicotiana benthamiana	N/A	N/A
Arabidopsis thaliana: WT col-0	N/A	N/A
Arabidopsis thaliana: *fer-4*	Tair (https://www.arabidopsis.org/)	GABI_106A06
Arabidopsis thaliana: *myc2*	Tair (https://www.arabidopsis.org/)	SALK_061267
Arabidopsis thaliana: *fer myc2*	This study	N/A
Arabidopsis thaliana: *MYC2-FLAGox*	This study	N/A
Arabidopsis thaliana: *MYC2^{A12}-FLAGox*	This study	N/A
Arabidopsis thaliana: *RALF23ox*	[37]	N/A
Arabidopsis thaliana: *fer RALF23ox*	This study	N/A
Arabidopsis thaliana: *FER-GFPox*	This study	N/A
Oligonucleotides		
Full list of oligonucleotides is presented in Table S3	N/A	N/A
Recombinant DNA		
pET42a GST	Novagen	Cat#70561
pET42a GST-MYC2	This study	N/A
pET42a GST-MYC2-N	This study	N/A
pET42a GST-MYC2-M	This study	N/A
pGEX-5X-1 GST	Sigma-Aldrich	Cat#GE28-9545-53
pGEX-5X-1 GST-FERK	This study	N/A
pMBP-H MBP	[40]	N/A
pMBP-H MBP-MYC2	This study	N/A
pMBP-H MBP-MYC2-N	This study	N/A
pMBP-H MBP-MYC2-M	This study	N/A
pMBP-H MBP-MYC2-C	This study	N/A
pMBP-H MBP-MYC2-NM	This study	N/A
pMBP-H MBP-MYC2-NM^{A12}	This study	N/A
pMBP-H MBP-FERK	This study	N/A
pYY384 BRI1P: FLAG	This study	N/A
pYY384 BRI1P:MYC2-FLAG	This study	N/A
pYY384 BRI1P:MYC2^{A12}-FLAG	This study	N/A
pYY46 35S:GFP	This study	N/A
pYY46 35S:FER-GFP	This study	N/A
pYY46 35S:FERm-GFP	This study	N/A
pYY361 BRI1P:c-MYC	[41]	N/A
pYY361 BRI1P:RALF23-c-MYC	[37]	N/A
pSKM660 S1P-YFP	[39]	N/A
pXY103 35S:YFPN	[41]	N/A
pXY103 35S: FERm-YFPN	This study	N/A
pXY104 35S:YFPC	[41]	N/A
pXY104 35S:MYC2-YFPC	This study	N/A
FERmiRNA	[16]	N/A

(*Continued on next page*)

Continued

REAGENT or RESOURCE	SOURCE	IDENTIFIER
Software and Algorithms		
JMP Pro	http://www.jmp.com	ver 12
R statistical package	http://www.rproject.org	ver 3.4.1
GeneOverlap	https://bioconductor.org/packages/release/bioc/html/GeneOverlap.html	ver 1.12.0
Venny	http://bioinfogp.cnb.csic.es/tools/venny/	ver 2.1.0

CONTACT FOR REAGANT AND RESOURCE SHARING

Further information and requests for resources and reagents should be directed to and will be fulfilled by the Lead Contact Yanhai Yin (yin@iastate.edu).

EXPERIMENTAL MODEL AND SUBJECT DETAILS

Plant Materials and Growth Conditions

The *Arabidopsis* accession Columbia-0 was used as WT in all experiments. T-DNA insertion mutants *fer*-4 (GABI_106A06) and *myc2* (Salk_061267), were obtained from the *Arabidopsis* Biological Resource Center (ABRC) [42], and homozygous lines were selected by genotyping (primers listed in Table S3). The *fer-4* mutant is referred as *fer* in this manuscript. The *fer myc2* double mutant was generated by crossing *fer* to *myc2*. *RALF23ox* was produced previously [37]. The *fer RALF23ox* was generated by crossing *fer* to *RALF23ox*. For all experiments involving *Arabidopsis* plants, seeds were sterilized with 70% ethanol containing 0.1% Triton and germinated on 1/2MS plates with 1% sucrose and 0.8% agar, with or without treatments as indicated when it is appropriate.

METHOD DETAILS

RNA-seq

For global gene expression profiling, 12-day-old seedlings were transferred to soil and grown at 22°C with 75% humidity under short day conditions, with an 8-hour light and 16-hour dark cycle in a growth chamber. After 3 more weeks, leaf tissues were collected and RNA was isolated using Trizol (Invitrogen) following the manufacturer's protocol. The RNA samples were then purified using RNeasy kit (QIAGEN) following the manufacturer's protocol. RNA-seq was performed at the DNA facility of Iowa State University with Illumina HiSeq 2000.

Bacterial pathogen growth and infiltration

Plants for the experiments were grown under same conditions as the ones for RNA-seq. Bacterial pathogen strains used in this study were *Pseudomonas syringae* pv. tomato (pst) DC3000 and the Coronatine deficient strain, pst DC3000 $^{COR-}$. The pst DC3000 was grown on plates with King's B medium containing 30ug/ml Rifampin at 28°C for 3 days before use, and pst DC3000 $^{COR-}$ grown under same condition with 100ug/ul Ampicillin in addition to Rifampin.

Bacterial pathogen accumulation experiments were done as described [43] with modifications. Briefly, pst DC3000 was scraped from the plate and resuspended in H2O, then diluted till the OD_{600} to 0.001 (about 10^6 colony forming unit or CFU/mL). The leaf infiltration was done with1 mL syringe without needle on the abaxial side of the leaf, usually 2-3 healthy and mature leaves per plant and 10-15 healthy plants were used per treatment. The infected plants were covered with a transparent plastic dome for 12 hr. Leaf discs (7mm in diameter) were collected with a hole puncher at indicated time points with 8-10 leaf discs per sample with three replicates per treatment. The leaf discs were ground in 0.5 mL sterile H2O, then the volume was brought up to 100 μl/disc with H2O, which was diluted serially (5 or10 times for each dilution with 5-6 dilutions). Aliquots (10 μl) of each dilutions were plated onto a grid of a gridded plate with King's B medium containing 30 μg/mL Rifampin and grown as described above. The numbers of bacterial colonies were counted and used to calculate the bacterial accumulation in plants (CFU/leaf disc). Statistical significance was calculated using Tukey HSD test. p values less than 0.05 were considered significant (Figures 1G and 1K). Statistical significance was calculated using Student's t test for Figures 4C, S3E, and S3G. The experiments are repeated more than three times and representative results are presented.

For MYC2 protein induction assay, pst DC3000 and pst DC3000 $^{COR-}$ were diluted to OD600 0.001 and 0.1, respectively, in H2O, and H2O only served as control. Leaves were collected at indicated times after infiltration for total or nuclear protein extraction, followed by western blotting.

Jasmonic acid treatment

For root growth inhibition assay, seeds of different genotypes were germinated on 1/2MS plates with 50 μm Jasmonic acid (Sigma) or control. The plates were kept at 4°C for 4 days and placed vertically for 7-8 days under constant light. About 12-18 representative seedlings from each genotype on JA or control plate were placed on a fresh 1/2MS plate and subjected to scanning.

For shoot growth assay, seeds of different genotypes were sterilized and spotted on gridded plate to better control the density and plates were kept at 4°C for 4 days and then placed horizontally under constant light. Plates with seedlings were scanned two weeks later.

For qPCR experiments, 10-day-old seedlings grown on 1/2MS plates were transferred to 1 mL liquid1/2MS medium in 24-well plates and incubated for 2 hr to minimize any mechanical touching effect. Then 1 mL liquid 1/2MS containing 100uM JA or control was added to each well, to make the final JA concentration 50uM. Three replicates for each treatment of each genotype were collected 10 hr after the treatment. RNA was extracted as described above, and qPCR was performed using SYBR Green PCR master mix (Applied Biosystems) on Stratagene Mx4000 real time PCR system.

Total protein and nuclear protein extraction

For total protein extraction from *Arabidopsis*, 100 mg tissues were collected and flash frozen in liquid nitrogen and ground directly in 300 μL 2xSDS sample buffer (100 mM Tris-Cl, pH6.8, 4% (w/v) sodium dodecyl sulfate, 0.2% (w/v) bromophenol blue, 20% (v/v) glycerol and 200 mM dithiothreitol) before SDS-PAGE and western blotting. For transient expression in *Nicotiana benthamiana*, 5 leaf discs (7mm in diameter) were collected for each sample and flash frozen in liquid nitrogen and ground directly in 200 μL 2xSDS sample buffer.

Nuclear protein extraction was carried out as described [44]. Briefly, half to one gram of tissue was collected and flash frozen in liquid Nitrogen and ground to powder. The sample powder was then resuspended in the lysis buffer (20mM Tris-HCl pH7.4, 25% Glycerol, 20mM KCl, 2mM EDTA, 2.5mM $MgCl_2$, 250mM Sucrose, 1mM DTT and 1mM PMSF added right before use), and filtered through 0.45um mesh to a new tube and spun for 10 min at 1500xg at 4°C. The pellet was resuspended in the nuclei resuspension buffer (20mM Tris-HCl pH7.4, 25% Glycerol, 2.5mM $MgCl_2$) with 0.2% Triton and spun for 10 min at 1500xg at 4°C. After two more washes, the nuclei were resuspended in the resuspension buffer without Triton and spun for 10 min at 1500xg at 4°C. The pellet was then resuspanded in 2xSDS buffer and used for western blotting. Nuclei from 1gram of tissue are resuspended in 100 μL 2xSDS buffer.

Protein half-life determination

This assay was carried out as described with modifications [45]. Briefly, seeds were germinated on 1/2MS plates vertically for 10 days. For WT and *fer*, seedlings were transferred to a 24-well plate containing 1/2MS liquid medium with 50 μM MG132, and gently shaken for 16 hr. The seedlings were rinsed with fresh 1/2MS liquid medium 5 times, and then supplied with fresh 1/2MS liquid medium containing 200 μM Cycloheximide (CHX), DMSO as control. For *MYC2-FLAGox* and $MYC2^{A12}$*-FLAGox*, *MYC2* was PCR amplified from *Arabidopsis* cDNA (Table S3) and $MYC2^{A12}$ was synthesized by GenScript (https://www.genscript.com) and the mutated codons are shown in Table S2. Both *MYC2* and $MYC2^{A12}$ were cloned to *pYY384 BRI1P:FLAG.* The transgenic seedlings were transferred to1 mL 1/2MS liquid medium and incubated for 2 hr to minimize any mechanical touching effect, and then 1 mL 1/2MS containing 400 μM CHX or DMSO control was added so the final CHX concentration is 200uM. Seedlings were collected at the time points indicated in Figures 2G, 3C, and 3D, and gently dabbed dry and flash frozen in liquid nitrogen. The samples were ground in 2xSDS sample buffer and used for western blotting. Protein half-life was estimated as the time when the protein level decreased to half of the amount of the control.

Transient expression assay in Nicotiana benthamiana (N. benthamiana)

N. benthamiana seeds were germinated in soil and the seedlings were transferred to soil in individual pots. About two-month-old plants were used for the assays. Agrobacterial cultures carrying the genes of interest were grown in liquid LB medium with antibiotics in a 30°C shaker for 2 days. The cultures were spun down in 1.5 mL microtubes at full speed for 1 min. The agrobacterium was resuspended in infiltration buffer (10mM $MgCl_2$, 10mM MES pH 5.7, 200 μM Acetosyringone). The density was measured at 600 nm wavelength and each agrobacterium was diluted to final concentration of OD600 0.3 for infiltration. The leaf infiltration was done with 1 mL syringe without needle on the abaxial side of the leaf.

Co-immunoprecipitation (CoIP)

FER was PCR amplified from *Arabidopsis* cDNA and cloned to pYY46 35S:GFP. FERm-GFP was generated using FER-GFP plasmid DNA with primers containing the mutation (Table S3). Agrobacteria carrying FERm-GFP and MYC2-FLAG were co-infiltrated to *N. benthamiana* leaves, co-infiltration of vector containing GFP only and MYC2-FLAG, vector containing FLAG only and FERm-GFP as controls. Leaf samples were collected two days after the infiltration. One gram of each sample was ground in liquid nitrogen and extracted with 2.5 mL IP buffer (10mM HEPEs pH7.5, 100mM NaCl, 1mM EDTA, 10% Glycerol, 0.5% NP-40) [41], with 1mM PMSF and one pellet of the protease inhibitor/10 mL from Roche. After 10 min rotation at 4°C, the mixture was centrifuged at 10,000 rpm for 10 min at 4°C and then filtered through two layers of Miracloth (Millipore). The IP was performed by adding 30 μL of GFP-TRAP-MA (Chromotek) to the filtered plant extract, rotated at 4°C for 2 hr. The IP product was precipitated using a magnetic stand after a brief spin at 1000xg for 1 min, and washed twice with IP buffer containing 0.5% NP-40 and twice with IP buffer without

NP-40. The IP product was resuspended in 2xSDS buffer and resolved on SDS-PAGE. Anti-GFP and anti-FLAG were used to detect FERm-GFP and MYC2-FLAG, respectively.

BiFC Assay

BiFC assay was conducted using the N-or C terminus of YFP [40] as described in [46]. FERm was subcloned to YFP-N upstream and MYC2 was subcloned to upstream of YFP-C and transformed into *Agrobacterium tumefaciens*. The different combinations of *Agrobacterium* (Figure 2D) were infiltrated into *N. benthamiana* leaves. After 48 hr, the YFP signal was detected using a Leica SP5 X MP confocal microscope with an HCS PL APO CS 20x0.7 oil objective. YFP was excited with a laser line of 514nm and detected from 530-560nm. Images were acquired with LAS AF software using identical settings for both specific interaction and controls.

Immunoprecipitation (IP) and *in vivo* phosphorylation detection

For MYC2 phosphorylation in *Arabidopsis*, 8 g of WT and 4 g of *fer* 4-week old plants were collected and ground in liquid nitrogen. IP was carried out using 50ul anti-MYC2 antibody in 20 mL IP buffer as described above, except that Halt protease and phosphatase inhibitor cocktail was used. 25ul Dynabeads Protein A (Invitrogen) was used to pull down anti-MYC2 antibody. Anti-MYC2 and Anti-phosphoserine (Sigma) were used to detect MYC2 and MYC2 phosphorylation, respectively.

For MYC2-FLAG and MYC2-FLAG^{A12} phosphorylation detection, the corresponding proteins were immunoprecipitated from transgenic plants 48 hr post pst DC3000 infection using anti-FLAG-M2 magnetic beads. About 1 g of leaf tissue of each genotype was collected, flash frozen and ground to powder. IP was carried out using anti-FLAG M2 magnetic beads in 2.5 mL IP buffer the same as described above, with 0.5% NP-40, 1mM PMSF and one pellet of the protease inhibitor/10 mL from Roche, for 2 hr. The beads were collected with a magnetic stand, and washed with 50mM HEPES pH 7.5 for 4 times. The beads were then resuspended in 100ul 1x phosphatase buffer (Roche). Half was taken to a new tube and 1.5ul phosphatase was added. The reactions were incubated at 37°C with rotation for 1 hr and stopped by adding 10ul 6xSDS buffer. The reactions were resolved on a Phos-tag gel and anti-MYC2 was used for western blotting.

For IP with anti-MYC2 from cytoplasmic proteins, pst DC3000-infiltrated leaves were collected and ground to powder in liquid nitrogen. Cytoplasmic protein was separated from non-cytoplasmic protein as described in the nuclear protein extraction. IP was carried out with the cytoplasmic portion, and the non-cytoplasmic portion was resuspended in 2XSDS buffer and used as control.

In vitro GST pull-down assay

GST pull-down assays were performed as described previously [45]. Briefly, FERK fused to glutathione-S- transferase (GST) on vector pGEX-5X-1, was purified using glutathione HiCap Matrix (QIAGEN). *MYC2, MYC2N, MYC2M, MYC2C* were PCR amplified from *MYC2-FLAG* plasmid DNA, cloned to pMBP-H and purified using amylose resin (NEB). All cloning primers are listed in Table S3. Approximately 2 μg of proteins were mixed into 1 mL of pull-down buffer (50mM Tris-HCl pH7.5, 200mM NaCl, 0.5% Triton X-100, 0.5mM β-mercaptoethanol, and protease inhibitors from Roche), and incubated at room temperature for 2 hr with rotation, then 10ul of GST beads (washed twice using the pull-down buffer) were added to each reaction and incubated under the same condition for another 2 hr. The GST beads were spun down, washed 5 times with the pull-down buffer, resuspended in 2XSDS buffer, resolved on 8% SDS-PAGE gel and detected by anti-MBP (NEB) antibody, 1% of each MBP fusion protein as input. The pull-down assays were repeated three times with similar results.

In vitro kinase assay and Mass Spectrometry to identify FER phosphorylation sites on MYC2

For *in vitro* kinase assays, *MYC2, MYC2N, MYC2M* were subcloned to pET42a. *MYC2NM* and *MYC2NM^{A12}* were PCR amplified from *MYC2-FLAG* and *MYC2A12-FLAG* plasmid DNA and cloned to pMBP-H vector (Table S3). GST, GST-MYC2, GST-MYC2N, GST-MYC2M (Figure 2E), MBP-MYC2NM and MBP-MYC2NM^{A12} (Figure 3A) proteins were mixed with GST-FERK in 20 μL kinase buffer (20 mM Tris, pH 7.5, 100 mM NaCl, 12 mM MgCl2 and 10 μCi ^{32}P-γATP) as previously described [47] and incubated at room temperature for 1 hr. The reactions were stopped by the addition of 2xSDS sample buffer and resolved on 8% SDS-PAGE. The phosphorylation was detected using phosphoimager. For the control for GST-FERK specificity, GST-MYC2M (Figure S2E) was mixed with GST or GST-FERK in kinase assay and phosphorylation detection was carried out as above.

Mass spectrometry analysis of phosphorylated proteins was carried out as described [46]. MBP-MYC2N and MBP-MYC2M were phosphorylated by GST-FERK in kinase buffer containing 10mM ATP. Reactions without GST-FERK were used as controls. Samples were subjected to protein digestion using Glu-C (ThermoFisher) and Trypsin (Roche) and LC-MS/MS performed using a Thermo Scientific Q-Exactive high-resolution quadrupole Orbitrap mass spectrometer. The raw data were extracted and searched against the TAIR10 proteome using Spectrum Mill v4.01 (Agilent Technologies). Phosphorylation sites were localized to a particular amino acid within a phosphopeptide using the variable modification localization (VML) score in Agilent's Spectrum Mill software [48].

Antibody Production

Anti-MYC2 was generated against MBP fusion protein with middle domain of MYC2 (amino acids 251-440, MBP-MYC2-M) and anti-FER was generated against MBP fusion protein with FERK domain (amino acids 470-895, pMBP-H MBP-FERK) in rabbits. Anti-MYC2 was purified with the corresponding GST fusion proteins (pET42a GST-MYC2-M) by affinity chromatography. The cloning primers are listed in Table S3.

QUANTIFICATION AND STATISTICAL ANALYSIS

RNA-seq data analysis

Raw RNA-seq reads were subjected to quality checking and trimming and then aligned to the *Arabidopsis* reference genome (TAIR10) using Genomic Short-read Nucleotide Alignment Program (GSNAP) [49]. The alignment coordinates of uniquely aligned reads for each sample were used to calculate the read depth of each annotated gene. These values were used to detect differential expression between WT and *fer* mutant samples. Two biological replicates were used for each genotype. The negative binomial QLSpline method implemented in the QuasiSeq package (http://cran.r-project.org/web/packages/QuasiSeq) was used to compute a p value for each gene with minimum one average read across all the samples in the comparison. The 0.75 quantile of reads from each sample was used as the normalization factor [50]. The adjusted p values (q-values) were converted from p values using a multiple test controlling approach [51, 52]. To control the false discovery rate at the 5% level, genes with q-values smaller than 0.05 were declared to be differentially expressed.

Venn diagrams were generated using Venny (http://bioinfogp.cnb.csic.es/tools/venny/).

Comparisons of hormone- [28, 31, 32] and *fer*-regulated genes were performed in R (version 3.3.0) using the *GeneOverlap* package (version 1.12.0; http://shenlab-sinai.github.io/shenlab-sinai/). p values for intersections between gene lists were assessed using Fisher's exact test and visualized with ComplexHeatmap. Clustering analysis of *fer* RNA-seq data was performed using the 'aheatmap' function of the NMF package in R (https://cran.r-project.org/web/packages/NMF/index.html) using log2 reads per million mapped reads (RPM) values. For identification of enriched promoter elements, 500bp promoter regions of the selected 1277 *fer*-regulated genes ($q < 0.05$ and >2-fold change), were bulk downloaded from TAIR and submitted to DREME [29] in the MEME Suite motif discovery (http://meme-suite.org/doc/dreme.html).

Root length measurement

The measurement of the root length was carried out using ImageJ. Statistical significance was calculated using Tukey HSD test. p values less than 0.05 were considered significant.

DATA AND SOFTWARE AVAILABILITY

The accession number for the raw RNA-seq data reported in this paper is SRA: PRJNA215313 (https://www.ncbi.nlm.nih.gov/bioproject?LinkName=biosample_bioproject&from_uid=2318105).

The mass spectrometry data is deposited to The MASSIVE database ftp://MSV000080972@massive.ucsd.edu with ID MSV000080972 and Password "MYC2." All other original data are available upon requests.